Analysis of optimal transport and related misfit functions in FWI

Yunan Yang and Björn Engquist, The University of Texas at Austin

SUMMARY

We summarize and compare four different misfit functions for full waveform inversion (FWI): the conventional least-squares norm, the integral wavefields misfit functional, the Normalized Integration Method (NIM) and the quadratic Wasserstein metric. The integral wavefields misfit functional and NIM are equivalent to the norm for Soblev space, which has intrinsic connections with the quadratic Wasserstein metric. We extract two important features of optimal transport. The first one is integration of data, which reduces high frequencies and globally compares observed and synthetic seismic waveforms. The other is rescaling of the data to be nonnegative. Numerical results illustrate that FWI with quadratic Wasserstein metric can effectively overcome the cycle skipping problem. A mathematical study on the convexity of the four misfit functions demonstrates the importance of data nonnegativity and integration in dealing with local minima in inversion.

INTRODUCTION

Full waveform inversion (FWI) is a data-driven method to obtain high resolution subsurface properties by minimizing the difference between observed and synthetic seismic waveforms (Virieux et al., 2017). In the past three decades, the least-squares norm (L^2) has been widely used as a misfit function (Tarantola and Valette, 1982; Lailly, 1983), which is known to suffer from cycle skipping issues with local minimum trapping and sensitivity to noise (Virieux and Operto, 2009). Other misfit functions proposed in literature, include the L^1 norm (Brossier et al., 2010), the Huber norm (Ha et al., 2009), filter based misifit functions (Warner and Guasch, 2014; Zhu and Fomel, 2016), seismic envelop inversion (Luo and Wu, 2015) and some others.

A recently introduced class of misfit functions are optimal-transport related (Engquist and Froese, 2014; Métivier et al., 2016; Engquist et al., 2016; Métivier et al., 2016; Yang et al., 2016). As useful tools from the theory of optimal transport, the quadratic Wasserstein metric (W_2) computes the optimal cost of rearranging one distribution into another with a quadratic cost function, while 1-Wasserstein metric (W_1) using absolute value cost function.

In this paper, we will also discuss about Normalized Intergration Method (NIM) which computes the least-squares difference between two normalized data sets (Liu et al., 2012; Chauris et al., 2012; Donno et al., 2013). If we consider the data are properly rescaled, the misfit of NIM is the norm of Sobolev space H^{-1} in mathematics. The connection between W_2 and H^{-1} is not obvious from the optimal transport definition, but is clear from the 1D closed solution formula. We shall also see that this is valid in higher dimensions even if there is no explicit solution formula.

The goal of this paper is to analyze important features of optimal transport and to compare with methods introduced earlier. We focus on two features in particular. One is integration of data and the other is the need to rescale the data to be nonnegative. Integration provides a global comparison between observed and synthetic data and also shifts the focus to lower frequencies. Nonnegativity further reduces the risk of cycle skipping.

THEORY

Full waveform inversion is a PDE-constrained optimization problem, minimizing the data misfit $d(f,g)$ by updating the model m, i.e. :

$$m^\star = \underset{m}{\operatorname{argmin}}\ d(f(x_r,t;m),g(x_r,t)), \tag{1}$$

where g is observed data, f is simulated data, x_r are receiver locations, and m is the model parameter. We get the modeled data $f(x,t;m)$ by solving a wave equation with a finite difference method (FDM) in both the space and time domain (Alford et al., 1974).

Generalized least squares functional is a weighted sum of the squared errors and hence a generalized version of the standard least squares misfit function. The formulation is

$$J_1(m) = \sum_r \int |W(f(x_r,t;m)) - W(g(x_r,t))|^2\, dt, \tag{2}$$

where W is an operator. In the conventioinal L^2 misfit, $W = I$, the identity operator.

The integral wavefields misfit functional (Huang et al., 2014) is a generalized least squares functional applied on full-waveform inversion (FWI) with weighting operator $W(u) = \int_0^t u(x,\tau)d\tau$. The objective function is defined as

$$J_2(m) = \sum_r \int \left| \int_0^t f(x_r,\tau;m)d\tau - \int_0^t g(x_r,\tau)d\tau \right|^2 dt, \tag{3}$$

If we define the integral wavefields $U(x,t) = \int_0^t u(x,\tau)d\tau$, then misfit function (3) is the ordinary least squares misfit between the observed and predicted integral wavefields $\int_0^t g(x_r,\tau)d\tau$ and $\int_0^t f(x_r,\tau;m)d\tau$. The integral wavefields still satisfy the original acoustic wave equation with a different source term: $\delta(\vec{x}-\vec{x}_s)\int_0^t s(\tau)d\tau = \delta(\vec{x}-\vec{x}_s)H(t)*s(t)$, where s is the original source term and $H(t)$ is the Heaviside step function (Huang et al., 2014).

Normalized Integration Method (NIM) is another generalized least squares functional, similar to the integral wavefields misfit functional. However, compared with integral wavefields misfit functional which directly integrates the observed and

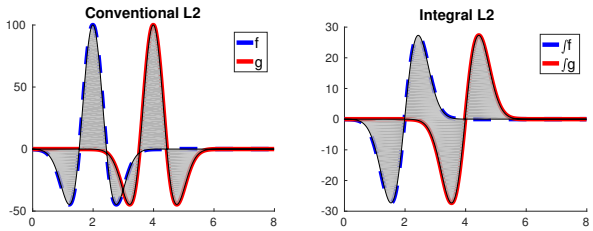

(a) Misfit for L^2 norm (b) Misfit for Integral L^2 method

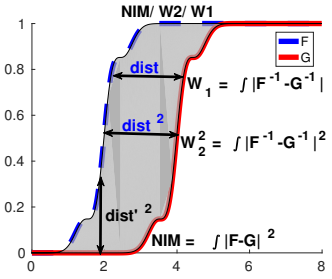

(c) Comparison among NIM, W_2, W_1 in 1D

Figure 1: The shaded areas represent the mismatch each misfit function considers. (a) L^2: $\int (f-g)^2 dt$. (b) Integral wavefields method: $\int (\int f - \int g)^2 dt$. After data normalization, (c) NIM measures $\int (F-G)^2 dt$, while W_2 considers $\int (F^{-1}-G^{-1})^2 dt$ and W_1 considers $\int |F^{-1}-G^{-1}| dt$.

synthetic data in time, NIM first preconditions the data and then takes the integration. The objective function is:

$$J_3(m) = \frac{1}{2}\sum_r \int |Q(f(x_r,t;m)) - Q(g(x_r,t))|^p \, dt, \qquad (4)$$

where Q is transformation of the wavefield u, defined as:

$$Q(u)(x_r,t) = \frac{\int_0^t P(u)(x_r,\tau)d\tau}{\int_0^T P(u)(x_r,\tau)d\tau}. \qquad (5)$$

The operator P is included to make the data nonnegative. Three common choices are $P_1(u) = |u|$, $P_2(u) = u^2$ and $P_3 = E(u)$, which correspond to the absolute value, the square and the envelop of the signal (Liu et al., 2012).

Despite the fact that both methods are measuring the L^2 misfit, there are three different features in NIM compared with conventional FWI. Data sets are normalized to be nonnegative, mass balanced and integrated in time. The first two are exactly the prerequisite of optimal transport based misfit functions, i.e. the Wasserstein metrics.

Optimal transport

Optimal transport refers to the problem of seeking the minimum cost required to transport mass of one distribution into another given a cost function, e.g. $|x-y|^p$. The mathematical definition of the distance between the distributions $f : X \to \mathbb{R}^+$ and $g : Y \to \mathbb{R}^+$ can then be formulated as

$$W_p^p(f,g) = \inf_{T_{f,g}\in\mathscr{M}} \int_X |x - T_{f,g}(x)|^p f(x)\,dx \qquad (6)$$

where $\mathscr{M}$ is the set of all maps $T_{f,g}$ that rearrange the distribution f into g (Villani, 2003).

The optimal transport formulation requires non-negative distributions and equal total masses, $\int f(x)dx = \int g(x)dx$, which are not natural for seismic signals. Therefore a proper data normalization is required before inversion. Datasets f and g can be rescaled to be nonnegative with values in range $[0,1]$, and to have equal mass. This step is exactly the same as the one in Equation (5) in NIM.

We can compare the data trace by trace and use the Wasserstein metric (W_p) in 1D to measure the misfit. The overall misfit is then

$$J_4(m) = \sum_{r=1}^{R} W_p^p(f(x_r,t;m), g(x_r,t)), \qquad (7)$$

where R is the total number of traces. In this paper, we mainly discuss the quadratic Wasserstein metric (W_2) when $p=2$ in (6) and (7).

PROPERTIES

Next we discuss the similarities and difference among the misfit functions mentioned above. We will regard f and g as the synthetic and observed data from one single trace as an 1D problem.

Relations among misfit functions

Conventional full-waveform inversion measures the L^2 norm difference $\int |f(t)-g(t)|^2 dt$, indicated by the shaded part in Figure 1a. The integral wavefields misfit functional first integrates f and g in time, and then measures their L^2 misfit (3). The integral wavefields can be viewed as wavefields produced by a low-passed seismic wavelet. The created lower frequency components (in Figure 1b) can properly explain the improvement in inversion (Huang et al., 2014).

With a proper normalization method, it is possible to scale the data to have nonnegativity and mass balance. This step is essential for both NIM and W_2. Since processing data trace-by-trace is an 1D problem, we are able to solve the optimal transport problem exactly (Villani, 2003). The optimal map is the unique monotone rearrangement of the density f into g. In order to compute the quadratic Wasserstein metric, we need the cumulative distribution functions F and G and their inverses F^{-1} and G^{-1}. The explicit formulation for the 1D Wasserstein metric is:

$$W_p^p(f,g) = \int_0^1 |F^{-1}(x) - G^{-1}(x)|^p dx. \qquad (8)$$

The interesting fact is that W_2 computes the L^2 misfit between F^{-1} and G^{-1} (Figure 1c), while the objective function of NIM measures the L^2 misfit between F and G, i.e. $\int_0^T |F(t)-G(t)|^2 dt$ (Figure 1c). This is identical to the mathematical norm of Sobolev space H^{-1}, $||f-g||^2_{H^{-1}}$, given f and g are nonnegative and sharing equal mass.

Since F and G are both monotone increasing, one can show that there is an equivalency between NIM and W_2 misfit with

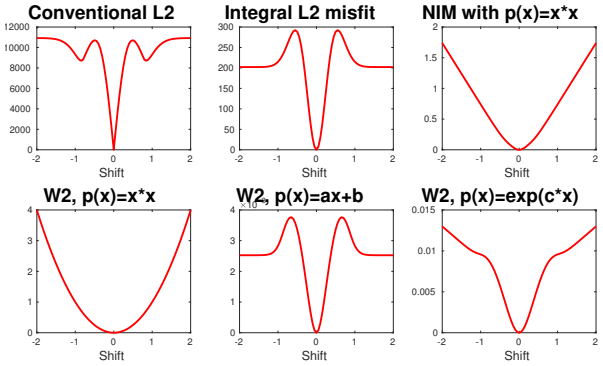

Figure 2: The misfit between $f(x)$ and $f(x-s)$ by six different misfit functions. First row shows conventional L^2 (left), intergral wavefield method (middle) and NIM with $p(x)=x^2$ (right). Second row shows the W_2 misfit with different normalization methods: $p(x)=x^2$ (left), $ax+b$ (middle) and $exp(c*x)$ (right).

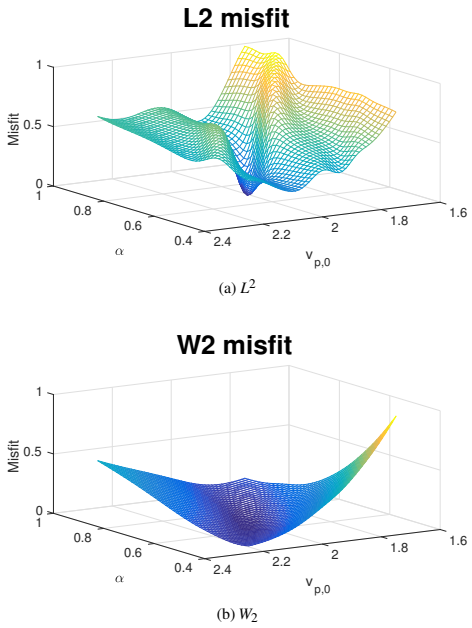

Figure 3: (a) Convexity plot of conventional L^2 (b) Convexity plot of trace-by-trace W_2 with normalization $p_2(x)=ax+b$

the same data normalization. Another demonstration of the similarity between NIM and optimal transport based metrics comes when $p=1$ in (4) and (8). These two misfits are the same since $\int|F(t)-G(t)|dt=\int_0^1|F^{-1}(x)-G^{-1}(x)|dx$.

Mathematical connection between H^{-1} norm and W_2 norm

Next we move into a general case that f and g are synthetic and observed data in higher dimensions, satisfying nonnegativity and conservation of mass. To compute the quadratic Wasserstein metric, we solve the following Monge-Ampère equation (Brenier, 1991)

$$\det(D^2u(x))=f(x)/g(\nabla u(x)) \tag{9}$$

If f and g are close enough and $g=(1+\varepsilon h+O(\varepsilon^2))f$, where h has mean zero, we can linearize (9) and also derive an approximation of the quadratic Wasserstein metric between f and g (Villani, 2003, p126-p127):

$$W_2^2(f,g)\approx\int_{\mathbb{R}^n}|\nabla\phi(x)|^2f(x)dx=||f-g||^2_{H^{-1}(d\mu)}, \tag{10}$$

where $d\mu=f(x)dx$. In one word, the quadratic Wasserstein metric is a weighted H^{-1} norm.

Besides, the dynamical characterization of the Wasserstein metric proposed by Benamou-Brenier (Benamou and Brenier, 2000) gives insights to consider that H^{-1} and W_2 belongs to the same class of measures. One can refer to Dolbeault et al. (2009) and Cardaliaguet et al. (2012) for more theoretical details, and Papadakis et al. (2014) for computational schemes. Mathematically, the misfits computed by NIM and W_2 are close also in higher dimensions.

Convexity

In order to illustrate the convexity of different objective functions, we borrow an example from Engquist and Froese (2014) that compares the misfit between a Ricker wavelet f and its shift $f(x-s)$. One can refer to the blue and red curves in Figure 1a. Here we plot the data misfits as a function of s in Figure 2. Conventional L^2, Intergral L^2 and NIM are compared on the first row. The second row displays W_2 misfits with three different scaling functions.

The figure on the top left for the conventional L^2 is the motivation of (Engquist and Froese, 2014) to bring the quadratic Wasserstein metric into seismic inversion. Such many local minima in the figure are not in favor of gradient-based optimization. The graph on the top middle is result of integral wavefields misfit functional. It creates lower frequency component, which decrease the chance of cycle skipping. Although having less local minima than conventional L^2, this method is still ill-posed in inversion. Integrating the wavefields or integrating the source may help invert the low wavenumber component of velocity, but still suffers from cycle skipping issues.

As demonstrated by Engquist et al. (2016), the squared Wasserstein metric has several properties that make it attractive as a choice of misfit function. One highly desirable feature is its convexity with respect to several parameterizations. However, the convexity highly depends on the data normalization method to satisfy nonnegativity and mass balance. The curves in the second row of Figure 2 are W_2^2 distance with different scaling functions: $p_1(x)=x^2$, and $p_2(x)=ax+b$ and $p_3(x)=\exp(c\cdot x)$. Theoretically p_1 gives perfect convexity, but having difficulty in inversion with adjoint-state method. From Taylor expansion p_3 is very close to p_2 when c is small, but easy to blow up with large c. Our current choice is to normalize data with p_2, but it is worth thinking a new normalization function that is able to preserve the convexity better.

It is interesting to compare the graph for NIM (upper right)

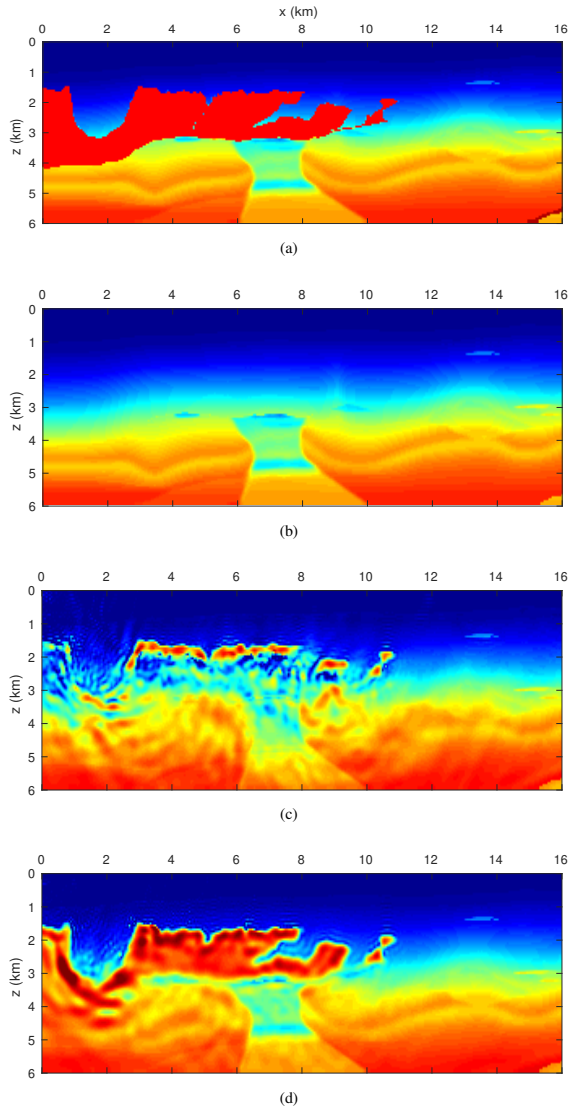

Figure 4: (a) True model velocity (b) Initial velocity (c) Inversion result using L^2 (d) Inversion result using W_2

with the one of W_2 (lower left) both of which are using the same normalization function (p_1) and globally convex with respect to the shift s. When $f(x)$ and $f(x-s)$ are close (i.e. $|s|$ is small), W_2 is a weighted H^{-1} as (10) states. Both curves have good convexity as $O(s^2)$ around zero. As $|s|$ gets larger, $W_2^2(f, f_s)$ is still $O(s^2)$, while the misfit measured by NIM is $O(s)$. The convexity of NIM becomes a bit weaker.

Finally we present a convexity result in model domain. We borrow the example from Métivier et al. (2016). The velocity model is assumed to vary linearly in depth as $v(x,z) = v_{p,0} + \alpha z$, where v_0 is the starting velocity on the surface, α is vertical gradient and z is depth. The reference for $(v_{p,0}, \alpha)$ is $(2km/s,\ 0.7s^{-1})$, and we plot the misfit curves with $\alpha \in [0.4, 1]$ and $v_0 \in [1.75,\ 2.25]$ on 41×45 grid in Figure 3. We observe many local minima and maxima in Figure 3a. Although W_2 is not convex in data domain with normalization method $p_2(x) = ax + b$ (Figure 2), the curve for W_2 (Figure 3b) is globally convex in model parameters $v_{p,0}$ and α. It demonstrates the capacity of W_2 in mitigating cycle skipping issues.

NUMERICAL EXAMPLE

In this section, we use a part of the BP 2004 benchmark velocity model (Billette and Brandsberg-Dahl, 2005) (Figure 4a) and an initial model without the upper salt part (Figure 4b) to do inversion with W_2 and L^2 norm respectively. A fixed-spread surface acquisition is used, involving 11 shots located every 1.6km on top. A Ricker wavelet centered on 5Hz is used to generate the synthetic data with a bandpass filter only keeping 3 to 9Hz components. We stopped the inversion after 300 L-BFGS iterations.

Here we precondition the data with function $p_2(x) = ax + b$ to satisfy the nonnegativity and mass balance in optimal transport. Inversion with trace-by-trace W_2 norm successfully construct the shape of the salt bodies (Figure 4d), while FWI with the conventional L^2 failed to recover boundaries of the salt bodies as shown by Figure 4c.

CONCLUSION

In this paper, we summarize and compare four misfit functions: the conventional least-squares inversion (L^2), the integral wavefields misfit function, the Normalized Integration Method (NIM), and the quadratic Wasserstein metric (W_2) from optimal transport. The L^2 norm is popular in general inverse problems, but suffers from cycle skipping in seismic inversion. The other three methods all incorporate the idea of integration the waveforms. Integration helps in enhancing the lower frequency component, but cannot avoid local minima coming from the oscillatory periodicity of the data. It is ideal to have a preconditioning operator which can "break" the periodicity and "record" the previous data information in time.

One solution is to combine the nonnegativity and integration in time together. Both NIM and the quadratic Wasserstein metric include these ideas as essential steps. A detailed discussion illustrates that the quadratic Wasserstein metric and the H^{-1} norm which NIM computes belong to the same family of mathematical measures. Moreover, H^{-1} and W_2 become equivalent when the two data sets are close. The analysis among these misfit functions of FWI brings additional insights into the importance of seismic data preconditioning, which also can be seen in examples of large scale FWI.

ACKNOWLEDGMENTS

We thank Sergey Fomel, Junzhe Sun and Zhiguang Xue for helpful discussions, and thank the sponsors of the Texas Consortium for Computational Seismology (TCCS) for financial support. This work was also partially supported by NSF DMS-1620396.

EDITED REFERENCES

Note: This reference list is a copyedited version of the reference list submitted by the author. Reference lists for the 2017 SEG Technical Program Expanded Abstracts have been copyedited so that references provided with the online metadata for each paper will achieve a high degree of linking to cited sources that appear on the Web.

REFERENCES

Alford, R., K. Kelly, and D.M. Boore, 1974, Accuracy of finite-difference modeling of the acoustic wave equation: Geophysics, **39**, 834–842, http://dx.doi.org/10.1190/1.1440470.

Benamou, J.-D., and Y. Brenier, 2000, A computational fluid mechanics solution to the monge-kantorovich mass transfer problem: Numerische Mathematik, **84**, 375–393, http://dx.doi.org/10.1007/s002110050002.

Billette, F., and S. Brandsberg-Dahl, 2005, The 2004 bp velocity benchmark: Presented at the 67th EAGE Conference & Exhibition.

Brenier, Y., 1991, Polar factorization and monotone rearrangement of vector-valued functions: Communications on pure and applied mathematics, **44**, 375–417, http://dx.doi.org/10.1002/(ISSN)1097-0312.

Brossier, R., S. Operto, and J. Virieux, 2010, Which data residual norm for robust elastic frequency-domain full waveform inversion?: Geophysics, **75**, no. 3, R37–R46, http://dx.doi.org/10.1190/1.3379323.

Cardaliaguet, P., G. Carlier, and B. Nazaret, 2012, Geodesics for a class of distances in the space of probability measures: Calculus of Variations and Partial Differential Equations, 1–26, https://doi.org/10.1007/s00526-012-0555-7.

Chauris, H., D. Donno, and H. Calandra, 2012, Velocity estimation with the normalized integration method: Presented at the 74th EAGE Conference and Exhibition incorporating EUROPEC 2012, https://doi.org/10.3997/2214-4609.20148721.

Dolbeault, J., B. Nazaret, and G. Savaré, 2009, A new class of transport distances between measures: Calculus of Variations and Partial Differential Equations, **34**, 193–231, http://dx.doi.org/10.1007/s00526-008-0182-5.

Donno, D., H. Chauris, and H. Calandra, 2013, Estimating the background velocity model with the normalized integration method: 75th Annual International Conference and Exhibition incorporating SPE EUROPEC, EAGE, Extended Abstracts, http://dx.doi.org/10.3997/2214-4609.20130411.

Engquist, B., and B. D. Froese, 2014, Application of the Wasserstein metric to seismic signals: Communications in Mathematical Sciences 12, https://doi.org/10.4310/cms.2014.v12.n5.a7.

Engquist, B., B. D. Froese, and Y. Yang, 2016, Optimal transport for seismic full waveform inversion: Communications in Mathematical Sciences, **14**, 2309–2330, http://dx.doi.org/10.4310/CMS.2016.v14.n8.a9.

Ha, T., W. Chung, and C. Shin, 2009, Waveform inversion using a back-propagation algorithm and a huber function norm: Geophysics, **74**, no. 3, R15–R24, http://dx.doi.org/10.1190/1.3112572.

Huang, G., H. Wang, and H. Ren, 2014, Two new gradient precondition schemes for full waveform inversion: arXiv preprint arXiv:1406.1864.

Lailly, P., 1983, The seismic inverse problem as a sequence of before stack migrations: Conference on inverse scattering: Theory and application: Society for Industrial and Applied Mathematics, 206–220.

Liu, J., H. Chauris, and H. Calandra, 2012, The normalized integration method-an alternative to full waveform inversion?: Presented at the 25th Symposium on the Application of Geophysics to Engineering & Environmental Problems, https://doi.org/10.3997/2214-4609.20144373.

Luo, J., and R.-S. Wu, 2015, Seismic envelope inversion: Reduction of local minima and noise resistance: Geophysical Prospecting, **63**, 597–614, http://dx.doi.org/10.1111/1365-2478.12208.
Métivier, L., R. Brossier, Q. Mérigot, E. Oudet, and J. Virieux, 2016, Measuring the misfit between seismograms using an optimal transport distance: Application to full waveform inversion: Geophysical Journal International, **205**, 345–377, http://dx.doi.org/10.1093/gji/ggw014.
Métivier, L., R. Brossier, Q. Mérigot, E. Oudet, and J. Virieux, 2016, An optimal transport approach for seismic tomography: application to 3d full waveform inversion: Inverse Problems, **32**, 115008, http://dx.doi.org/10.1088/0266-5611/32/11/115008.
Papadakis, N., G. Peyré, and E. Oudet, 2014, Optimal transport with proximal splitting: SIAM Journal on Imaging Sciences, **7**, 212–238, http://dx.doi.org/10.1137/130920058.
Tarantola, A., and B. Valette, 1982, Generalized nonlinear inverse problems solved using the least squares criterion: Reviews of Geophysics, **20**, 219–232, http://dx.doi.org/10.1029/RG020i002p00219.
Villani, C., 2003, Topics in optimal transportation: American Mathematical Society, Graduate Studies in Mathematics 58.
Virieux, J., A. Asnaashari, R. Brossier, L. Métivier, A. Ribodetti, and W. Zhou, 2017, In 6. An introduction to full waveform inversion: Encyclopedia of Exploration Geophysics, R1-1–R1-40, http://dx.doi.org/10.1190/1.9781560803027.entry6.
Virieux, J., and S. Operto, 2009, An overview of full-waveform inversion in exploration geophysics: Geophysics, 74, no. 6, WCC1–WCC26, http://dx.doi.org/10.1190/1.3238367.
Warner, M., and L. Guasch, 2014, In Adaptive waveform inversion: Theory: 84th Annual International Meeting, SEG, Expanded Abstracts, 1089–1093, http://dx.doi.org/10.1190/segam2014-0371.1.
Yang, Y., B. Engquist, J. Sun, and B.-D. Froese, 2016, Application of optimal transport and the quadratic wasserstein metric to full-waveform inversion: arXiv preprint arXiv:1612.05075.
Zhu, H., and S. Fomel, 2016, Building good starting models for full-waveform inversion using adaptive matching filtering misfit: Geophysics, 81, no. 5, U61–U72, http://dx.doi.org/10.1190/geo2015-0596.1

Full waveform inversion with an exponentially-encoded optimal transport norm

*Lingyun Qiu *, Jaime Ramos-Martínez and Alejandro Valenciano, PGS; Yunan Yang and Björn Engquist, University of Texas at Austin*

Summary

Full waveform inversion (FWI) with L^2 norm objective function often suffers from cycle skipping that causes the solution to be trapped in a local minimum, usually far from the true model. We introduce a new norm based on the optimal transport theory for measuring the data mismatch to overcome this problem. The new solution uses an exponential encoding scheme and enhances the phase information when compared with the conventional L^2 norm. The adjoint source is calculated trace-wise based on the 1D Wasserstein distance. It uses an explicit solution of the optimal transport over the real line. It results in an efficient implementation with a computational complexity of the adjoint source proportional to the number of shots, receivers and the length of recording time. We demonstrate the effectiveness of our solution by using the Marmousi model. A second example, using the BP 2004 velocity benchmark model, illustrates the benefit of the combination of the new norm and Total Variation (TV) regularization.

Introduction

FWI is formulated as a nonlinear inverse problem matching modeled data to the recorded field data (Tarantola, 1984). Usually, a least-square objective function is used for measuring the data misfit. This misfit is minimized with respect to model parameter and the model update is computed using the adjoint state method. FWI can produce high-resolution models of the subsurface when compared to ray-based methods. Due to the large scale of the problem, local rather than global optimization methods are mandatory. However, FWI is often an ill posed problem due to the band-limited nature of the seismic data and the limitations of the acquisition geometries. Furthermore, the non-convexity resulting from the least-square objective function causes the local minima, i.e., cycle-skipping problem, especially with data lacking low frequency information.

It is well known that the least-square formulation of FWI tends to produce many local minima. This is because only the pointwise amplitude difference is measured with L^2 norm while the phase or travel-time information embedded in the data is more critical for the inversion. There are different approaches proposed to capture the travel-time difference, such as dynamic time warping and convolution based methods. This information is used in order to convexify the objective function or enlarge the true solution valley. In this direction, we mention the works in (Luo and Sava, 2011), (Ma and Hale, 2013) and (Warner and Guasch, 2014).

Recently, the Wasserstein distance has been proposed to replace the L^2 distance for the objective function in FWI (Engquist and Froese, 2014). The Wasserstein distance is a well-defined metric from the theory of optimal transport in mathematics. It was first brought up by Gaspard Monge in 1781 (Monge, 1781) and more recently by Kantorovich (Kantorovich, 1942) seeking the optimal cost of rearranging one density into the other, where the transportation cost per unit mass is the Euclidean distance or Manhattan distance.

Wasserstein distance has the ability to consider both phase shifts and amplitude differences It has been demonstrated in (Engquist, Froese and Yang, 2016) that W^2 bears some advantageous mathematical properties, such as convexity with respect to shift and dilation and insensitivity to noise. In (Yang Engquist, Sun and Froese 2016), W^2 on 2D data is applied to FWI on synthetic benchmark models. The calculation of the corresponding adjoint source requires solving a Monge–Ampère equation that can be computationally demanding. Another popular optimal transport metric used for FWI is the 1-Wasserstein distance (W^1), approximated by the Kantorovich Rubinstein (KR) norm (Métivier, et al, 2016). For this metric the transport map is not unique. The KR norm doesn't require data to be positive and mass preserved. Therefore it can be directly applied to the seismic data without transferring them into probability density function (pdf). Both analysis and numerical results shows the potential of FWI with optimal transport to mitigate cycle-skipping problem.

The Wasserstein metric is designed to measure the distance between two pdfs. Thus, non-negativeness and unit mass are desired for the input. But, oscillation and sign-change are typical features of the seismic data. Therefore, we need a misfit function that takes the global features of data into consideration and is robust to periodicity and sign-change. Since seismic data are not naturally positive, a proper normalization method is the key to Wasserstein distance based inversion. Some previous methods may lead to non-differentiable misfit function and are not compatible with adjoint-state method, or lose information of original data during the normalization.

Here, we address the issue of how to transform seismic data into pdfs. The new solution uses an exponential encoding scheme and enhances the phase information when compared with the conventional L^2 norm. The algorithm

uses of the 1D Wasserstein metric. As a result, the implementation of the adjoint source has the same order of computational complexity as of the conventional L^2 norm. We illustrate our method by using the Marmousi and the BP 2004 velocity benchmark models.

Exponentially-encoded Wassesrtein distance for seismic data

In this section, we define a procedure to transfer the seismic data into pdf-like data before we calculate the Wasserstein distance between them. Meanwhile, we also pursue to extract the phase information from the seismic data for computing Wasserstein distance. Seismic data are not naturally positive, which is a challenge to apply W^2 directly. Some previous methods such as comparing the positive and negative parts separately (Engquist and Froese, 2014) seem not be compatible with adjoint-state method. The linear transformation (Yang Engquist, Sun and Froese, 2016) may lose the global convexity that W^2 has for positive signals. Therefore a proper data normalization method is the key for inversion.

Suppose we have seismic data d, which has both positive and negative values. We let

$$\tilde{d} = e^{\alpha d}$$

where α is a prescribed positive constant to control the upper bound of the power for the numerical accuracy. Since the exponential function has the feature that it has much milder derivative on the negative half real axis, the above procedure treat the negative and positive part of the seismic data differently. At the same time, the processed data is non-negative. We apply this procedure to both the recorded data and simulation with the same constant. With an additional scaling, we turn the recorded data d and simulated data u into pdf-like functions $\tilde{\boldsymbol{d}}$ and $\tilde{\boldsymbol{u}}$. Therefore, we can apply the Wasserstein distance to measure their difference.

Intuitively, the above algorithm is nothing but an uneven encoding process. All the information in the positive part of the data is amplified and stored in $(\mathbf{1}, +\infty)$ and the information from the negative part is compressed in $(\mathbf{0}, \mathbf{1})$. In this way, the phase information is extracted mainly from the positive side of the seismic data for the FWI. This encoding process is invertible and Fréchet differentiable. Therefore, according to the chain rule, the only additional work is to multiply the adjoint source by

$$\frac{\partial \tilde{d}}{\partial d} = \alpha e^{\alpha d}.$$

FWI with this encoding process will be biased to match travel-time provided by the positive signal. The negative side is also needed, especially for FWI with reflection data. To make use of the phase information from the negative part of the data, we balance this uneven encoding by also taking into account the data reformed by the map

$$\tilde{d} = e^{-\alpha d}.$$

In practice, we perform the inversion in an alternative fashion. That is, we switch the data encoding process between $\tilde{d} = e^{\alpha d}$ and $\tilde{d} = e^{-\alpha d}$ every few iterations.

The corresponding objective function is constructed as

$$J = \sum_{shot} \sum_{receiver} W_2^2(\tilde{u}, \tilde{d}).$$

Since we only change the objective function, the corresponding modification for the conventional FWI is to use a new adjoint source. It can be computed as

$$\frac{\partial J}{\partial u} = \sum_{shot} \sum_{receiver} \left(\frac{\partial}{\partial \tilde{u}} W_2^2(\tilde{u}, \tilde{d}) \frac{\partial \tilde{u}}{\partial u} \right).$$

Note that $\tilde{d}$ and $\tilde{u}$ are 1D functions. We can take advantage of the explicit expression of the Wasserstein distance for distributions over the real line. In this way, the computational complexity for obtaining the adjoint source is $O(N_r N_s N_t)$, where N_r, N_s and N_t stand for the number of receivers, shots and time steps, respectively. In practice, we find that the additional computational time is very small compared with the conventional method to calculate the adjoint source, which is a subtraction with the same order of complexity $O(N_r N_s N_t)$.

The quadratic Wasserstein distance between two 1D pdfs p_0 and p_1 is defined as

$$\begin{aligned} W_2^2(p_0, p_1) &= \int_0^1 (f_0^{-1}(s) - f_1^{-1}(s))^2 ds \\ &= \int_0^1 (f_0^{-1}(f_1(t)) - t)^2 p_1(t) dt \end{aligned}$$

Here, f_0 and f_1 are the associated cumulative distribution functions (cdf) and $\cdot^{-1}$ stands for the pseudo-inverse defined as

$$f^{-1}(t) = \inf\{s \mid f(s) > t\}.$$

The Fréchet derivative with respect to p_1 is given by

$$\frac{\partial W_2^2(p_0, p_1)}{\partial p_1} =$$

$$(f_0^{-1}(f_1(t)) - t)^2 + \int_t^1 2 \frac{\partial f_0^{-1}(x)}{\partial x} |_{x=f_1(s)} (f_0^{-1}(f_1(s)) - s) p_1(s)\, ds.$$

The above equality can be simplified using the inverse function theorem and we have that

$$\frac{\partial W_2^2(p_0, p_1)}{\partial p_1} =$$

$$(f_0^{-1}(f_1(t)) - t)^2 + 2 \int_{f_0^{-1}(f_1(t))}^1 (s - f_1^{-1}(f_0(s)))\, ds.$$

Note that both f_0 and f_1 are monotonic increasing functions. Hence, $f_0^{-1}(f_1(t))$ and $f_1^{-1}(f_0(t))$ are computed in $O(N_t)$ operations and both are monotonic functions. Therefore, we can obtain the adjoint source for a single trace with $O(N_t)$ operations. Once the adjoint source is obtained, the rest of the inversion is the same as the conventional FWI.

Numerical experiments

We first investigated the use of our method on the Marmousi model (Figure 1a). The model contains many reflectors, steep dips, and strong velocity variations in both the lateral and the vertical direction. The velocity model is 9.2 km × 3.2 km. The synthetic data was created with a minimum frequency of 5 Hz (zero power) and 7 Hz full power. The sources and receivers are both uniformly distributed every 20 m at 40 m depth. The maximum recording time is 8 s. We randomly select 31 sources per iteration. The initial model (Figure 1b) is created by smoothing the true model using a Gaussian filter with 2 km correlation length. With this initial model, inversion with $\boldsymbol{L^2}$ objective function fails to provide a good reconstruction (Figure 1c) but the $\boldsymbol{W^2}$ gives a result closer to the true model (Figure 1d).

Next, we perform numerical test on the BP 2004 benchmark velocity model (Figure 2a) (Billette and Brandsberg-Dahl, 2005). The model is 28.5 km × 7.5 km and contains a salt body in the middle of the domain of interest. The synthetic data was created with a minimum frequency of 1 Hz (zero power) and 3 Hz full power. For the acquisition geometry, the sources are uniformly distributed every 40 m and the receivers are deployed every 40 m with a maximum offset of 20 km. Both source and receiver are located at 40m depth. With this long-offset setting, the maximum recording time of the data is set to 12 s. For efficiency purpose, a random selected 36 shots are used per iteration.

A heavily smoothed model (1.1 km correlation length) from the true model with the water layer fixed is used as the starting velocity model for FWI (Figure 2b). From this initial model, the conventional FWI with L^2 distance fails to recover the salt boundary (Figure 2c). As shown in Figure 2d, inversion with proposed algorithm produces better reconstruction. The salt body shallower than 7 km depth is well restored. Slices of initial model, true model, L^2 reconstructed model and W^2 reconstructed model at x=12 km are shown in Figure 3.

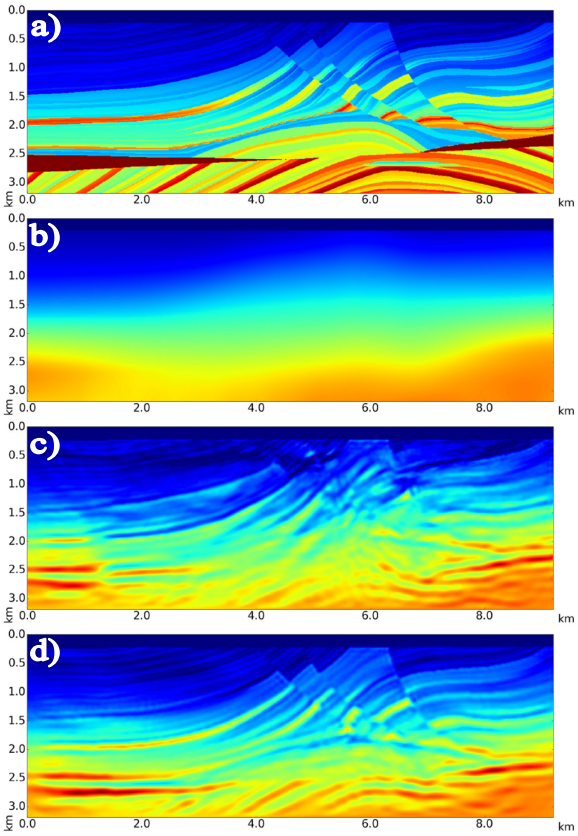

Figure 1: (a): True model, (b) Initial model, (c) FWI with $\boldsymbol{L^2}$ (d) FWI with $\boldsymbol{W^2}$.

In this work, we focus on measuring the difference in data space. Thus, no conditioning or stabilization procedure, such as smoothing on the gradient and regularization on the model, is applied to the inversion results shown in Figure 2 and 3.

The oscillatory noise in FWI can be efficiently removed using total variation type regularization (Qiu, et al., 2016). The regularization is necessary to stabilize the inversion and inject a priori information into the optimization. The extension of the proposed algorithm to incorporate TV regularization is straightforward. The inversion results are shown in Figure 4 and 5. The TV regularization helps to produce a blocky inverted model. But, from the slices view (Figure 5), it is clear that the FWI with $\boldsymbol{L^2}$ distance (blue curve) and TV regularization do not restore the salt boundary correctly. In contrast, the $\boldsymbol{W^2}$ model is close to the true model showing almost perfect sediment velocity and salt boundary reconstruction.

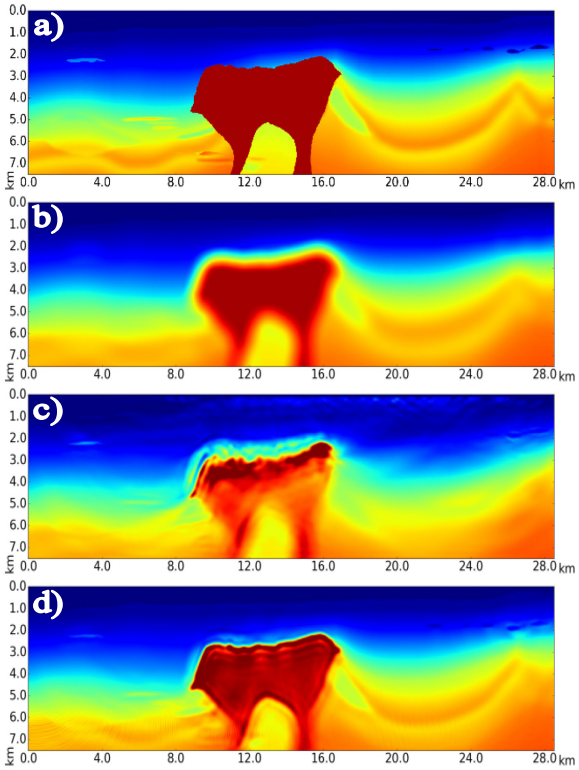

Figure 2: (a): True model, (b) Initial model, (c) FWI with $\boldsymbol{L^2}$ (d) FWI with $\boldsymbol{W^2}$.

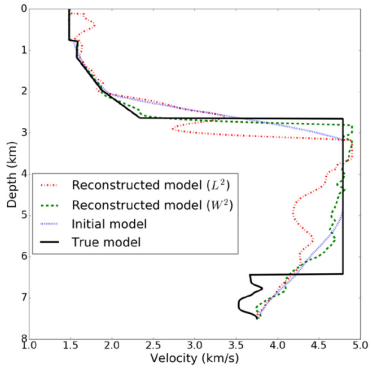

Figure 3: Slices of the velocity models in Figure 2.

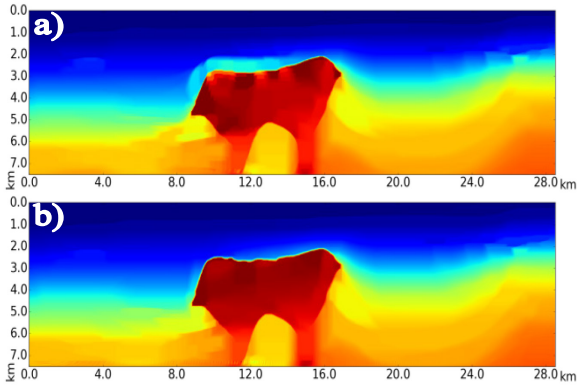

Figure 4: (a): $\boldsymbol{L^2}$ with TV regularization, (b): $\boldsymbol{W^2}$ with TV regularization

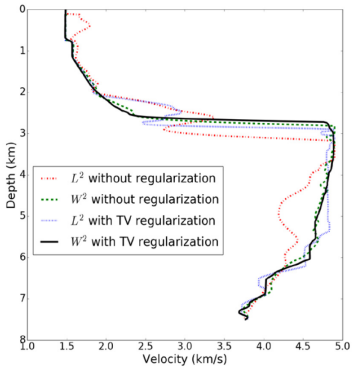

Figure 5: Slices of the velocity models with TV regularization in Figure 4.

Conclusions

The formulation of FWI with Wasserstein distance shows the potential to mitigate the cycle-skipping problem present in the $\boldsymbol{L^2}$ solution. We propose an exponential-encoding process to transfer the seismic data into pdf with emphasis on phase information. The adjoint source is calculated using the explicit solution of the optimal transport over the real line. All the efforts lead to an efficient and robust seismic inversion scheme. The numerical results demonstrate the advantages of the proposed algorithm. In the Marmousi example the new method allows the FWI to start from a heavily smoothed model with high frequency data and obtain a good result. The BP 2004 benchmark example shows how by combining the new norm with TV regularization the salt body velocity and boundaries can be reconstructed starting from a smooth model.

Aknowledgments

We thank PGS for permission to publish the results.

EDITED REFERENCES

Note: This reference list is a copyedited version of the reference list submitted by the author. Reference lists for the 2017 SEG Technical Program Expanded Abstracts have been copyedited so that references provided with the online metadata for each paper will achieve a high degree of linking to cited sources that appear on the Web.

REFERENCES

Billette, F. J., and S. Brandsberg-Dahl, 2005, The 2004 bp velocity benchmark: 67th Annual International Conference and Exhibition, EAGE, Extended Abstracts.

Ramos-Martinez, J., S. Crawley, S. Kelly, and B. Tsimelzon, 2011, Full-waveform inversion by pseudo-analytic extrapolation: 81st Annual International Meeting, SEG, Expanded Abstracts, http://dx.doi.org/10.1190/1.3627750.

Tarantola, A., 1984, Inversion of seismic refection data in the acoustic approximation: Geophysics, **49**, 1259–1266, http://doi.org/10.1190/1.1441754.

Engquist, B., and B. D. Froese, 2014, Application of the Wasserstein metric to seismic signals: Communications in Mathematical Sciences, **12**, 979–988, http://dx.doi.org/10.4310/CMS.2014.v12.n5.a7.

Engquist, B., B. D. Froese, and Y. Yang, 2016, Optimal transport for seismic full waveform inversion: Communications in Mathematical Sciences, **14**, 2309–2330, http://dx.doi.org/10.4310/CMS.2016.v14.n8.a9.

Yang, Y., B. Engquist, J. Sun, and B. D. Froese. Application of optimal transport and the quadratic wasserstein metric to fullwaveform inversion, arXiv preprint arXiv:1612.05075, 2016.

Metivier, L., R. Brossier, Q. Merigot, E. Oudet, and J. Virieux, 2016, Measuring the mis t between seismograms using an optimal transport distance: application to full waveform inversion: Geophysical Journal International, **205**, 345–377.

Warner, M., and L. Guasch, 2014, Adaptive waveform inversion: Theory: 84th Annual International Meeting, SEG, Expanded Abstracts, 1089–1093, http://dx.doi.org/10.1190/segam2014-0371.1.

Luo, S., and P. Sava, 2011, A deconvolution-based objective function for wave-equation inversion: 81st Annual International Meeting, SEG, Expanded Abstracts, 2788–2792, http://dx.doi.org/10.1190/1.3627773.

Ma, Y., and D. Hale, 2013, Wave-equation refection traveltime inversion with dynamic warping and full-waveform inversion: Geophysics, 78, R223-R233, https://doi.org/10.1190/geo2013-0004.1.

Monge, G., 1781, Memoire sur la theorie des deblais et des remblais: Del'Imprimerie Royale.

Kantorovich, L. V., 1942, On the translocation of masses: In Dokl. Akad. Nauk SSSR, **37**, 199–201.

Qiu, L., N. Chemingui, Z. Zou, and A. Valenciano, 2016, Full-waveform inversion with steerable variation regularization: 86th Annual International Meeting, SEG, Expanded Abstracts, 1174–1178, http://dx.doi.org/10.1190/segam2016-13872436.1.